Research Square

Preprints are preliminary reports that have not undergone peer review.
They should not be considered conclusive, used to inform clinical practice,
or referenced by the media as validated information.

Thermal Kinetic Modelling and Experimental Performance of Enzymatic Nanocellulose–Reinforced Sustainable Natural Rubber Nanocomposites

M P Poornima
St. Joseph's College
M Roshna
St. Joseph's College
P Dileep
Rubber Park India (P) Ltd
Sinto Jacob
sintojacob@staloysiuselt.edu.in
St. Joseph's College

Research Article

Keywords: Biomaterials, Nanocomposites, Thermal modelling, Kinetics analysis

Posted Date: September 14th, 2026

DOI: https://doi.org/10.21203/rs.3.rs-10849110/v1

License: This work is licensed under a Creative Commons Attribution 4.0 International License.
Read Full License

Additional Declarations: No competing interests reported.

Thermal Kinetic Modelling and Experimental Performance of Enzymatic Nanocellulose–Reinforced Sustainable Natural Rubber Nanocomposites

Poornima M P[1,2], Roshna M[3], Dileep P[4], Sinto Jacob*[1,5]

[1]Department of Chemistry, St. Joseph's College, Irinjalakuda, Thrissur, Kerala, India

[2]Department of Chemistry, Sree Sankara Vidyapeetom College, Valayanchirangara, Kerala, India

[3]Department of Chemistry, St. Joseph's College, Devagiri, Kozhikode, Kerala, India

[4] JJ Murphy Research Centre, Rubber Park India (P) Ltd., Valayanchirangara, Kerala, India

[5]Department of Chemistry, St. Aloysius College, Elthuruth, Thrissur, Kerala, India

*Corresponding author:

E-mail address: sintojacob@staloysiuselt.edu.in

Abstract

The growing demand for sustainable, non-toxic, renewable, and environmentally friendly materials is particularly crucial in bio-related applications. Natural fiber–reinforced elastomeric composites hold significant potential in this regard. In the present study, dry natural rubber (DNR) was reinforced with enzymatic nanocellulose (NC), to prepare sustainable nanocomposites. A comprehensive characterization of the resulting nanocomposites was performed, including morphological analysis, curing behavior, thermal stability, mechanical performance, and other physical properties. The DNR/NC-2 composite exhibited a 15.5% increase in tensile strength and a 23% improvement in tear strength compared to DNR/NC-0. Additionally, DNR/NC-5 demonstrated a 38% enhancement in tensile modulus. Thermogravimetric analysis (TGA) revealed enhanced thermal stability, particularly for the DNR/NC-2 composite, which exhibited an increase of approximately 8°C in degradation temperature. The elevated tan δ values in DNR/NC-2 at both 0 °C and 60 °C suggest enhanced wet-skid performance and a marginal rise in rolling resistance. The activation energy (E_a) determined using the Flynn–Wall–Ozawa (FWO), Kissinger–Akahira–Sunose (KAS), Friedman, and Vyazovkin methods exhibited strong correlation. The DNR/NC-2 composite showed the highest E_a, compared to the DNR/NC-0 and DNR/NC-5 composite, thereby proving its better thermal stability. The observed variation in E_a as conversion progresses demonstrated the multi-step degradation kinetics. Notably, these improvements were achieved without surface modification of the NC, emphasizing its potential as a bio-based reinforcing filler for the development of sustainable elastomeric nanocomposites.

Keywords: *Biomaterials; Nanocomposites; Thermal modelling; Kinetics analysis*

1. Introduction

Polymer nanocomposites have emerged as promising materials due to their significant scientific relevance and broad industrial applications [1]. The incorporation of nanoscale fillers has gained widespread acceptance in the development of high-performance elastomeric nanocomposites, offering enhanced functionality and greater design flexibility [2]. Rubber, with its high extensibility and elasticity, is a versatile material widely used across industries such as aerospace, automotive, and agriculture [3]. Natural rubber (NR), composed primarily of *cis*-1,4-polyisoprene constitutes the bulk of commercial elastomeric materials [4]. Due to its regular molecular structure, NR exhibits excellent tensile strength, flexibility, resilience, and low heat buildup. However, NR is rarely used in its raw form. To tailor its performance for specific applications, it is typically compounded with various additives, such as fillers, vulcanizing agents, and antioxidants [5]. These additives improve properties such as mechanical strength, environmental durability, hardness, and processability. Fillers, in particular, play a key role by either enhancing performance or reducing production costs [6]. Their reinforcing effect results from the partial immobilization of polymer chains, which reduces slippage and increases mechanical strength.

Traditional fillers include carbon black (CB), silica, kaolin, and synthetic fibers [7]. However, with the growing global emphasis on environmental sustainability, there has been a shift toward the development and use of eco-friendly, bio-based fillers. Biofillers such as cellulose, starch, lignin, chitin, pectin, and alginates have been investigated for their ability to enhance elastomeric performance while being environmentally benign [8]. Among these, cellulose is one of the most abundant and renewable natural polymers [9]. As a primary structural component of plant cell walls, it can be extracted from sources such as wood, grasses, seed fibers, algae, fungi, bacteria, and even marine organisms [10]. Due to its biodegradability, non-toxicity, renewability, colloidal stability, and cost-effectiveness, cellulose has long been utilized in industries including food, pharmaceuticals, textiles, and coatings, and it continues to play a vital role in the development of bio-based products [11].

Nanocellulose (NC) derived from native cellulose, retains biocompatibility while exhibiting superior physical properties and unique surface chemistry [12]. Both cellulose nanofibrils (CNFs) and cellulose nanocrystals (CNCs) are collectively referred to as "nanocelluloses" [13].

In recent years, NC has gained significant attention due to its anisotropic morphology, renewability, excellent mechanical performance, surface functionalization potential, biocompatibility, and optical clarity [14]. NC has a high surface area enriched with hydroxyl groups, which allows for extensive surface modification [15]. It also possesses one of the highest specific strengths among biopolymers and features a distinctive three-dimensional network structure. For instance, CNFs - due to their high aspect ratio - offer enhanced reinforcement and fracture toughness compared to conventional fillers, which typically exhibit globular or plate-like morphologies [16]. Moreover, CNFs are capable of strong interfacial interactions with natural rubber and, in some cases, can form covalent bonds without prior surface modification, making them highly suitable for reinforcing elastomers in sustainable nanocomposite applications. Dominic et al. highlighted that the combined use of CB and NC derived from rice husk offers a significant advancement in creating eco-friendly Natural Rubber nanocomposites with improved performance characteristics, making them well-suited for green tire technologies [17]. Koeipudsa et al. reported improved mechanical and thermal properties in NR composites reinforced with CNCs extracted from oil palm trunk biomass [18]. Suppanucharoen et al. developed an eco-friendly natural rubber–cellulose sponge composite exhibiting excellent mechanical strength and high water absorption efficiency [19].

NC was obtained in this research from the leaves of *Acalypha hispida* through enzymatic hydrolysis using xylanase, an enzyme derived from the bacterium *Bacillus pumilus* [20]. The extracted NC was incorporated into DNR to develop nanocomposites. The influence of NC on the cure characteristics, mechanical strength, thermal stability, dynamic mechanical behavior, and barrier properties of DNR vulcanizates was thoroughly investigated, with NC acting as the reinforcing phase. This study contributes to addressing pressing global challenges by reducing reliance on non-renewable synthetic materials and promoting sustainable, environmentally friendly alternatives.

2. Experimental

2.1. Materials

Natural rubber (ISNR-5) with a Plasticity Retention Index (PRI) of 60 was supplied by the Rubber Research Institute of India, Kottayam, Kerala**.** Stearic acid**,** zinc oxide**,** tetramethylthiuram disulfide (TMTD)**,** N-cyclohexyl-2-benzothiazole sulfenamide (CBS)**,** tetramethyl quinoline (TMQ)**,** and sulfur were procured from Associated Rubber Chemicals

Pvt. Ltd., Kochi, India**.** NC with a particle size of 30–40nm, was extracted from A. hispida leaves using a green enzymatic hydrolysis method with xylanase, as per protocols reported in our previous work [20].

2.2. Methods

2.2.1. Composite preparation

The raw rubber was first masticated at a rotor speed of 30rpm for 2min to soften it. This was followed by the addition of all compounding ingredients, except for the accelerators and vulcanizing agents, which were mixed thoroughly for 3min. The remaining curatives were then added, and mixing continued for another 2min to ensure uniform dispersion. After compounding, the mixture was passed through a laboratory two-roll mill (6″×12″) five times, with the nip gap gradually widened from a tight setting to 3mm to produce uniform sheets. The resulting rubber compound was then conditioned at room temperature for 24h prior to moulding. The formulation details for the DNR nanocomposites are given in Table 1. The composites were labelled as DNR/NC-0 (containing no NC) and DNR/NC-1 through DNR/NC-5, representing NC loadings of 1, 2, 3, 4, and 5phr, respectively.

Table 1. Formulation of DNR/NC compounds

Ingredients [a] **(phr)** [b]	Names of DNR/NC compounds					
	DNR/NC-0	**DNR/NC-1**	**DNR/NC-2**	**DNR/NC-3**	**DNR/NC-4**	**DNR/NC-5**
DNR	100	100	100	100	100	100
NC	0	1	2	3	4	5

[a] Zinc oxide 5.0, stearic acid 2.0, TMD 1.0, N-cyclohexyl-2-benzothiazole sulphenamide 0.6, Tetramethyl thiuram disulphide 0.2, and sulphur 2.5 were common to all mixes.

[b] parts per hundred of rubber

2.2.2 Characterization methods

Fourier Transform Infrared (FTIR) spectra of the composites were recorded in the range of 4000–400cm^{-1} using a Thermo Nicolet Avatar 370 FTIR spectrophotometer**.** The morphological characteristics of the composites were examined using a Zeiss Sigma Field Emission Scanning Electron Microscope (FE-SEM) operating at an acceleration voltage of 3kV**.** Thermal stability was assessed via thermogravimetric analysis (TGA) under a nitrogen atmosphere**,** across a temperature range of 28°C to 750°C**,** at a heating rate of 20°C/min**.** Dynamic mechanical properties were evaluated using a Dynamic Mechanical Analyzer (DMA

Q800, TA Instruments) with a temperature sweep from –80°C to 80°C, a heating rate of 3°C/min, and a constant frequency of 1Hz. The curing behavior of the composites was analyzed using a Rubber Process Analyzer (RPA 2000) in accordance with ASTM D5289. Tensile properties were measured using a Universal Testing Machine (Instron) as per ASTM D412, while tear strength was evaluated following ASTM D624. To assess the effects of thermal aging, samples were placed in a hot air oven at 70°C for 72h, after which their mechanical properties were re-evaluated. Hardness was tested using a Shore A Durometer in accordance with ASTM D2240. Abrasion resistance was determined using a Bareiss DIN Abrader following ASTM D5963, and specific gravity was measured with a densimeter as per ASTM D297. The compression set of vulcanized samples was evaluated according to ASTM D395, while heat build-up was measured using a Goodrich Flexometer (Dynisco, USA) based on ASTM D623. Rebound resilience was tested using a Dunlop Tripsometer, in accordance with ASTM D7121. Flex cracking and crack growth behavior were studied using a Dematttia Flexing Machine, with flex cracking tested as per ASTM D430 and crack growth as per ASTM D813. Swelling behavior was evaluated using toluene as the solvent, and crosslink density was calculated using the Flory–Rehner equation. Tribological properties, including coefficient of friction and specific wear rate, were measured using a pin-on-disc tribometer at ambient temperature, according to ASTM G99-05. Thermal conductivity was assessed using Holmarc's Lee's Disc Apparatus (Model: HOAE-LD18) following the ASTM D7340 standard.

Kinetic analysis

TG analysis was performed under a nitrogen atmosphere using heating rates of 5, 10, 15, and 20℃ to study their thermal decomposition behaviour. The resulting weight loss data were subsequently analyzed using NETZSCH's Kinetics Neo software. This software employed several model-free isoconversional methods-specifically KAS, FWO, Friedman, and Vyazovkin-to determine the activation energy and the pre-exponential (Arrhenius frequency) factor (A) across the thermal degradation process. This approach is advantageous for characterising complex, multistep degradation processes because it calculates E_a and A at various degrees of conversion (α= 0.1 to 0.8) without relying on a pre-assumed reaction model.

The equation given below can represent the kinetics involved in TGA

$$d\alpha/dt = k(T)f(\alpha) \text{--------(1)}$$

Where α indicates the degree of sample conversion, f(α) shows the weight loss change of the sample undergoing disintegration, k signifies the rate constant, and t is the time interval. It was also possible to relate the rate constant with the E_a requirement using the following equation

$$k=Ae^{\frac{-Ea}{RT}} \text{--------(2)}$$

Here A refers to the pre-exponential factor (s^{-1}), E_a denotes the activation energy (J/mol), R represents to the universal gas constant (8.314 J/mol K), and T stands for temperature (K). α can be evaluated as per the following equation

$$\alpha = \frac{W_0 - W_t}{W_0 - W_f} \text{-------(3)}$$

here w_o indicates the weight of the sample before degradation, w_t indicates the weight of the sample that is undergoing degradation at time t w_f is the weight of the residue. The predicted E_a was found to following the same trends using these models.

Flynn–Wall–Ozawa (FWO) method

The FWO integral model, widely adopted for estimating thermal kinetic parameters, links E_a with the biomass heating rate and the inverse of temperature based on the original approach proposed by Doyle.

$$\log(\beta) = log\left(\frac{AE_a}{Rg(\alpha)}\right) - 2.315 - \frac{0.4567E_a}{RT} \text{ ---------- (4)}$$

Here $g(\alpha)$ = decomposition mechanism

The E_a is obtained from the slope of the straight-line plot of log β versus 1/T.

Kissinger–Akahira–Sunose (KAS) method

Pyrolysis kinetics can be estimated using the widely applied model-free KAS method, as expressed in Eq. (5), where the E_a at each conversion level is obtained from the slope of the plot of ln (β/T^2) versus 1/T.

$$\ln\left(\frac{\beta}{T^2}\right) = \ln\left(\frac{AR}{E_a g(\alpha)}\right) - \left(\frac{E_a}{RT}\right) \text{ ----------(5)}$$

Vyazkovin method

E_a is also determined using the Vyazovkin method, a nonlinear and isoconversional approach that primarily depends on the operating temperature and the extent of conversion, as represented in Eq. (6).

$$\int_0^{\alpha} \frac{dy}{f(y)} = A \int_0^{t} e^{(-E_a/RT)dt} \quad \text{---------- (6)}$$

Friedman method

The Friedman method is a differential isoconversional technique that does not rely on integral approximations; at a given conversion level (α), plotting ln(dα/dT) against 1/T produces a straight line whose slope ($-E_a/R$) is used to determine the activation energy.

$$ln\left(\frac{d\alpha}{dT}\right) = ln[Af(\alpha)] - \frac{E_a}{RT} \quad \text{---------- ---------(7)}$$

3. Results and Discussion

3.1 Cure characteristics of DNR composites

Table 2 Cure properties of DNR composites

Sample name	Cure time (min)	Scorch time (min)	Differential torque (dNm)
DNR/NC-0	3.08	1.5	7.94
DNR/NC-1	3.10	1.5	8.06
DNR/NC-2	3.19	1.6	8.19
DNR/NC-3	3.44	1.5	8.36
DNR/NC-4	3.17	1.5	8.36
DNR/NC-5	2.94	1.4	8.47

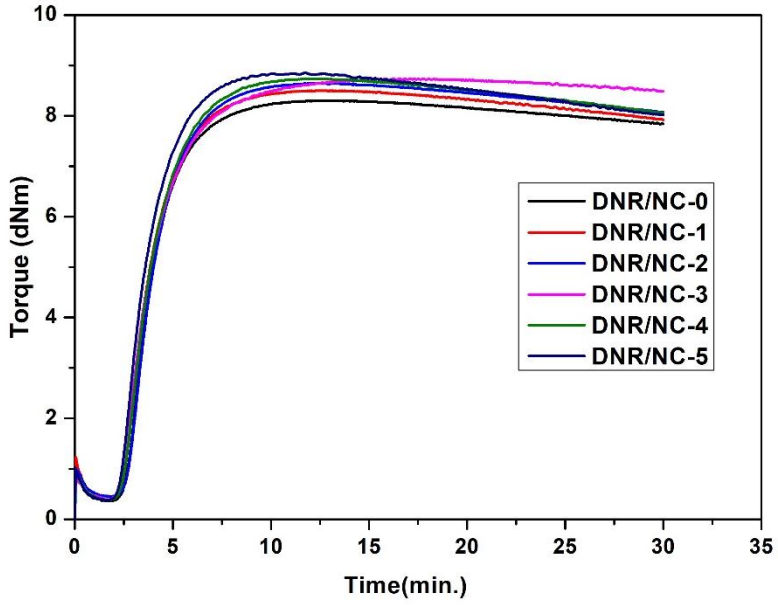


Fig.1 Cure curves of DNR composites

Fig.1 displays the cure curves of DNR composites with varying loadings of NC fibres, and the corresponding data are presented in Table 2. The cure time increases up to DNR/NC-3, likely due to moderate levels of NC inhibiting vulcanization through curative adsorption. At higher NC loadings, filler agglomeration reduces effective interaction with curing agents, resulting in a shorter cure time [21]. Torque values exhibit a consistent increase up to DNR/NC-5 due to the enhanced stiffness and reinforcing effect of NC, which increases the material's resistance to deformation during curing [22]. Scorch time remains relatively consistent across all DNR/NC samples, indicating that NC has minimal influence on the initial stage of vulcanization.

3.2 Mechanical characterisations

3.2.1 Stress-strain properties

The mechanical performance of the DNR composites was evaluated using tensile test data presented in Table 3, with corresponding stress–strain curves shown in Fig.2. The DNR/NC-2 composite exhibited a 15.5% increase in tensile strength compared to DNR/NC-0, attributed to the reinforcing effect of NC fibrils. These fibrils facilitate stress transfer to the rubber matrix through strong interfacial interactions. However, beyond the optimum NC loading, tensile strength decreased, likely due to fibril agglomeration, which disrupts uniform dispersion and introduces stress-concentrating defects [23]. Such agglomerates compromise the mechanical integrity of the composite by hindering effective stress transfer. The incorporation of NC also led to a reduction in elongation at break, most likely due to restricted mobility of the polymer chains [24]. Notably, the DNR/NC-2 composite showed a 23% improvement in tear strength, while the DNR/NC-5 composite exhibited a 38% increase in tensile modulus at 500% elongation compared to DNR/NC-0. This increase in modulus at higher NC content is attributed to enhanced stiffness provided by the cellulose fibrils, which reinforce the composite structure [25]. At elevated NC levels, stronger interactions between cellulose and the rubber matrix improve load-bearing capacity and deformation resistance, resulting in greater rigidity and tensile modulus. The resulting stiffness contributes to improved dimensional stability under mechanical loading.

Table 3 Mechanical characteristics of DNR composites

Sample name	Tensile strength (MPa)	Elongation at break (%)	Modulus at 500% elongation (MPa)	Tear strength (N/mm)
DNR/NC-0	23.71±0.6	674±10	9.67±0.04	45.13±2.4
DNR/NC-1	25.59±0.4	670±10	10.60±0.06	49.30±3.8
DNR/NC-2	27.38±0.5	651±14	12.31±0.05	55.40±0.5
DNR/NC-3	25.15±0.6	646±10	12.12±0.07	55.40±0.6
DNR/NC-4	24.06±0.5	632±17	12.35±0.03	52.36±1.5
DNR/NC-5	22.84±1.2	611±22	13.33±0.07	50.45±1.6

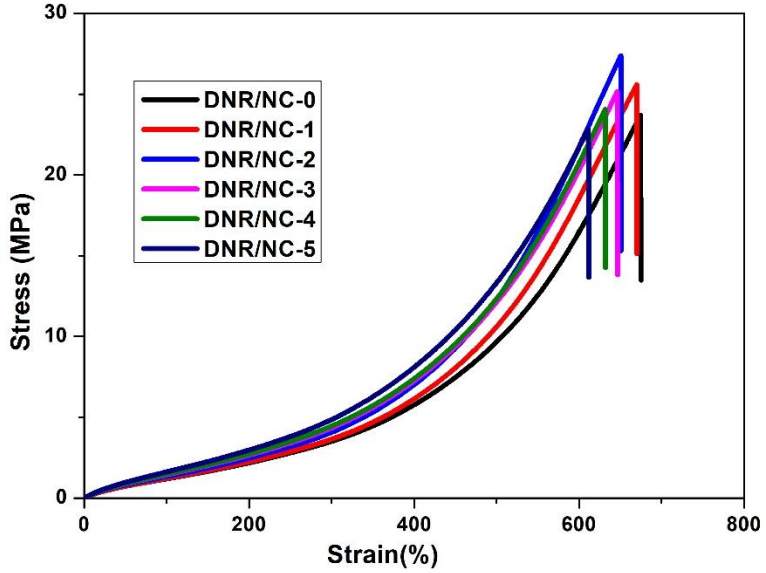


Fig.2 Stress-strain curves of DNR composites

3.2.2 Ageing studies

Fig.3 shows the tensile retention percentages of DNR composites after aging. Following the aging process, a decrease in tensile strength was observed, mainly due to oxidative degradation and chain scission within the DNR matrix. These degradation effects weaken the interfacial adhesion between the cellulose and the rubber matrix, thereby reducing the overall tensile performance of the composites. However, all DNR composites retained more than 90% of their original tensile strength, with the lowest retention observed in DNR/NC-0 [26]. While a slight increase in tensile retention was noted at lower NC loadings, a sharp decline occurred at higher concentrations, likely due to agglomeration that adversely affects retention. The tensile retention trends are consistent with thermal analysis results, further supporting the indication of thermal stability in the composites.

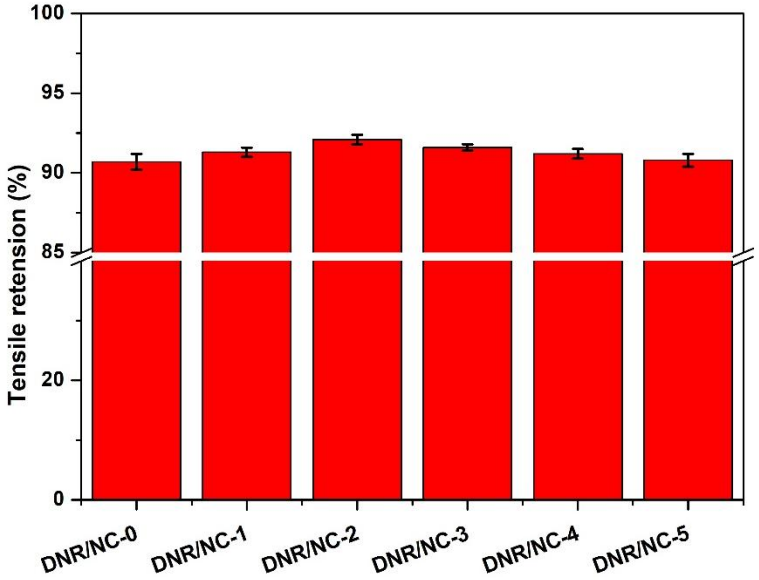


Fig.3 Variation in the tensile retention percentage with increasing fibre content

3.2.3 Flexural strength

Table 4 Flexural characteristics of DNR composites

Sample name	Crack initiation (Kilocycles)	Crack propagation (Kilocycles)
DNR/NC-0	38	98
DNR/NC-1	43	120
DNR/NC-2	53	151
DNR/NC-3	50	144
DNR/NC-4	52	149
DNR/NC-5	50	138

Flex cracking and crack growth resistance are critical dynamic properties for rubber products intended for demanding, dynamic applications which is presented in Table 4. In DNR composites, these properties primarily depend on filler dispersion**,** crosslink network structure**,** filler loading, and the presence of antidegradants, which influence mechanical-oxidative aging [27,28]. An improvement in resistance to flex cracking and crack growth was observed up to the DNR/NC-2 composite, likely due to better dispersion of NC and enhanced crosslinking. However, at higher NC loadings, a decline in resistance was noted, attributed to **NC** agglomeration and rigid interactions with the NR matrix, leading to stress concentration and reduced flexibility.

3.2.4 Specific gravity

Table 5 Specific gravity of the DNR composites

Sample name	DNR/ NC-0	DNR/ NC-1	DNR/ NC-2	DNR/ NC-3	DNR/ NC-4	DNR/ NC-5
Specific gravity	0.98	1.00	1.02	1.04	1.05	1.07

The specific gravity values of the vulcanized samples are presented in Table 5. A slight increase in specific gravity was observed in the DNR composites compared to the DNR/NC-0 sample. This increase is primarily due to the incorporation of fillers and additives, which have a higher density than DNR. Their contribution to the overall mass per unit volume of the composites accounts for the recorded rise in specific gravity [29].

3.2.5 Technological characteristics

Table 6 Technological properties of the DNR/NC composites

Sample name	Heat buildup (°C)	Rebound resilience (%)	Abrasion resistance index (%)	Compression set (%)	Hardness (Shore A)
DNR/NC-0	1	75.74 ±2	54.64±3	18.6±0.5	41±1
DNR/NC-1	2	72.44±2	62.69±2	19.7±1	43±1
DNR/NC-2	3	70.10±2	81.69±3	20.6±0.5	44.5±1
DNR/NC-3	4	68.20±2	78.56±3	22.1±1	45.5±1
DNR/NC-4	5	66.79±1	76.11±5	23.4±1	46±1
DNR/NC-5	7	65.86±1	67.04±7	25.7±1	48.5±1

Table 6 outlines the key technological characteristics of the DNR/NC composites. Rebound resilience is defined as the ratio of energy recovered after deformation to the energy initially applied to cause the deformation. In DNR-NC composites, rebound resilience decreases progressively from the DNR/NC-0 to the DNR/NC-5 formulation. This reduction is attributed to the incorporation of NC particles, which enhance the stiffness and rigidity of the polymer matrix, thereby negatively affecting its resilience [30]. The addition of NC enhances the abrasion resistance of natural rubber. Among the composites, DNR/NC-2 exhibited the lowest volume loss, indicating the highest abrasion resistance, as abrasion resistance increases with decreasing volume loss. The improved performance is attributed to the increased crosslink

density of the DNR/NC-2 composite. However, beyond a filler loading of 3phr NC, the abrasion resistance index decreases due to the agglomeration of filler particles [31]. Compression set is the permanent deformation retained by a material after being subjected to compressive stress for a specified duration and temperature. In DNR–NC composites, compression set values increase with higher NC content, primarily due to the added rigidity imparted by the filler and the resulting decrease in the material's elastic recovery [32].

Hardness refers to a material's ability to resist reversible deformation under the application of a rigid indenter. The Shore A hardness values for DNR/NC-0 and the DNR/NC-5 composite are 41 and 48, respectively. This increase in hardness results from the uniform distribution of NC fibers within the DNR matrix, which enhances its rigidity [33]. The improved stiffness is attributed to the formation of a three-dimensional NC network, facilitated by extensive inter- and intramolecular hydrogen bonding. Additionally, stronger interfacial adhesion between NC and the DNR matrix further contributes to the increased hardness and stiffness. Heat build-up is the amount of heat generated and dissipated during the cyclic deformation of a material. In DNR composites, heat build-up increases from 1°C in DNR/NC-0 to 7°C in the DNR/NC-5 composite [34]. This increase is primarily due to greater friction—both between fillers and at the rubber–filler interface. As the NC content rises, repeated compression under dynamic loading causes continuous breakage and reformation of filler agglomerates, which further elevates internal friction and consequently contributes to heat build-up.

3.2.6 Tribology of DNR composites

The friction coefficients of DNR/NC-0 and DNR/NC-2 composites were experimentally determined, as shown in the corresponding Fig.4. The COF for DNR/NC-0 was higher than that of the DNR/NC-2 composite. This property is influenced not only by the size of the filler particles but also by their structural characteristics [35]. Abrasion resistance generally improves in composites with higher modulus and lower friction coefficients [36]. This trend aligns well with the observed abrasion resistance behaviour of the DNR composites. The specific wear rate of DNR/NC-0 is higher than that of the DNR/NC-2 composite, primarily due to its lower interfacial bonding and overall inferior wear resistance which is shown in Fig.5.

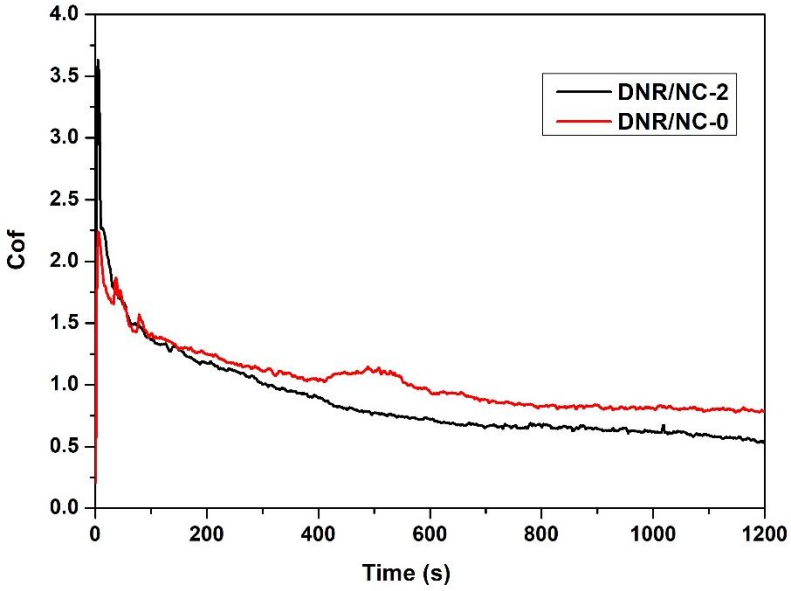


Fig.4 Coefficient of Friction of DNR/NC-0 and DNR/NC-2 composite

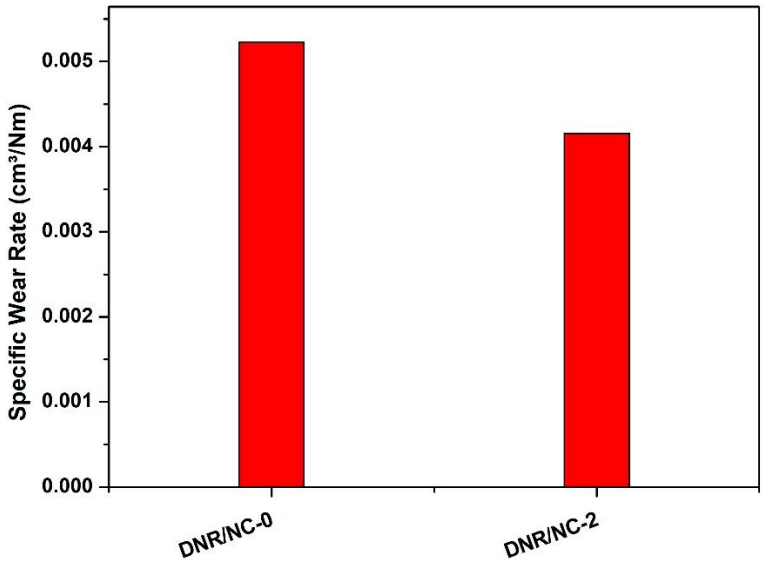


Fig.5 Specific wear rate of DNR/NC-0 and DNR/NC-2 composite

3.2.7 Thermal conductivity of DNR composites

The thermal conductivity values for DNR/NC-0 and DNR/NC-2 composite are shown in the Fig.6. Compared to DNR/NC-0, the DNR/NC-2 composite exhibits slightly higher thermal conductivity. This enhancement is attributed to the presence of NC, which introduces limited thermal conduction pathways and facilitates improved energy transfer within the matrix [37].

Nonetheless, both materials remain low in overall thermal conductivity, characteristic of insulating polymers.

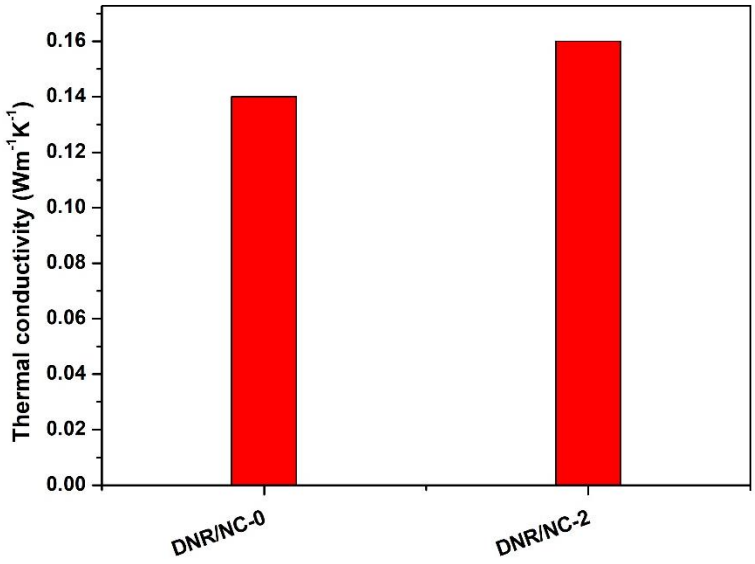


Fig.6 Thermal conductivity of DNR/NC-0 and DNR/NC-2 composite

3.2.8 FESEM analysis

Fig.7 presents the FESEM micrographs of the tensile fracture surfaces of the DNR/NC-0 and DNR/NC-2 composites. The DNR/NC-0 sample exhibits a relatively flat and smooth fracture surface, whereas the DNR/NC-2 composite shows a coarse and irregular surface with visible NC fibrils [38]. Most of these nanofibers are well dispersed within the DNR matrix, although some small agglomerates are also observed. The increased surface roughness indicates strong interfacial bonding between the NC and the rubber matrix. This enhanced interaction contributes to the improved mechanical performance of the DNR/NC-2 composite.

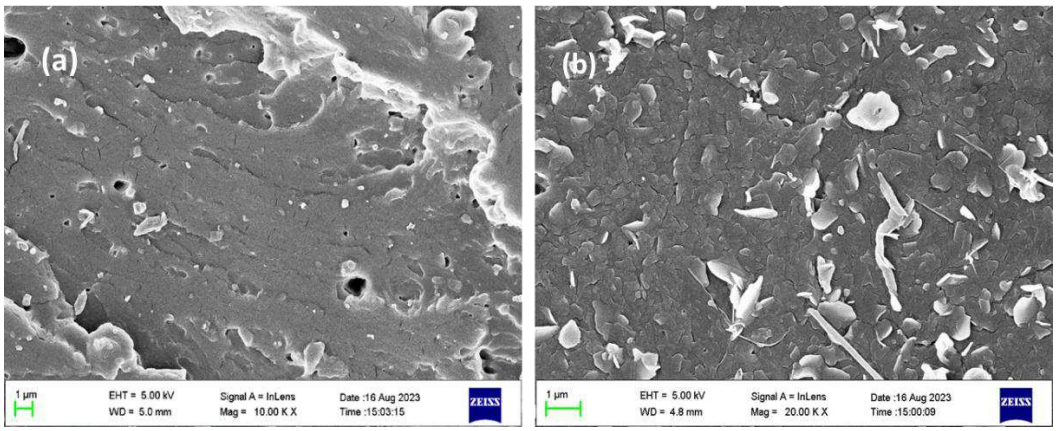


Fig.7 FESEM micrographs of (a) DNR/NC-0 and (b) DNR/NC-2 composite

3.2.9 FTIR analysis

FTIR spectra of DNR/NC-0 and DNR/NC-2 composites are presented in Fig.8. In DNR/NC-0, the peaks at 2957, 2914, and 2852 cm^{-1} correspond to $–CH_3$ asymmetric stretching, $–CH_2$ asymmetric stretching, and $–CH_2$ symmetric stretching, respectively [39]. The absorption at 1658 cm^{-1} arises from C=C stretching vibrations in the polyisoprene backbone. Additionally, the bands at 1444 and 1371 cm^{-1} indicate $–CH_2$ and $–CH_3$ bending modes, while the peak at 830 cm^{-1} is attributed to =C–H out-of-plane bending. Compared to DNR/NC-0, the FTIR spectrum of the DNR/NC-2 composite shows notable differences, confirming the incorporation of NC into the matrix. A broad band near 3300 cm^{-1} appears, corresponding to O–H stretching vibrations from the hydroxyl groups of NC, indicating strong hydrogen bonding [40]. The C–H stretching and bending bands (2957, 2914, 2852, 1444, and 1371 cm^{-1}), along with the C=C vibration at 1658 cm^{-1}, become broader, reflecting increased matrix rigidity due to the presence of NC. The =C–H bending peak at 830 cm^{-1} appears sharper, suggesting better dispersion and interfacial interaction between NC and the DNR matrix. Furthermore, peaks in the 1020–1150 cm^{-1} region become significantly sharper, corresponding to glycosidic linkages and C–O–C stretching vibrations from NC.

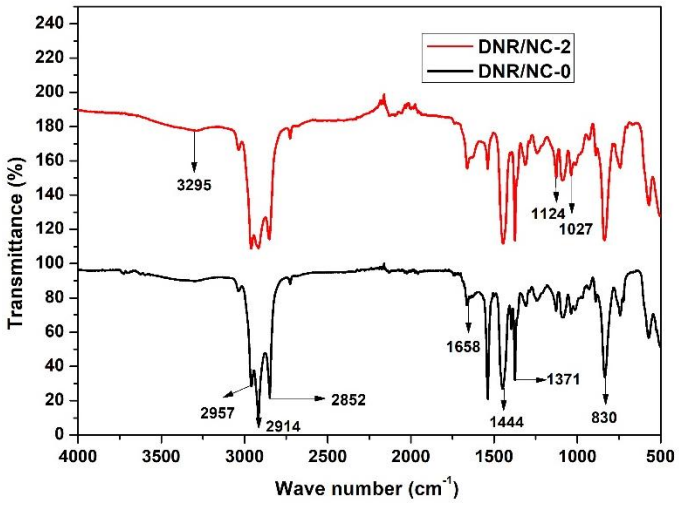


Fig.8 FTIR profiles of (a) DNR/NC-0 and (b) DNR/NC-2 composite

3.2.10 Dynamic Mechanical analysis

The dynamic mechanical characteristics of NC-reinforced NR vulcanizates were evaluated over a temperature range using DMA. This method provides insights into the viscoelastic behavior of the polymer and is also employed to assess the extent of interaction between the rubber matrix and the filler. Fig. 9 presents the variation in storage modulus, loss modulus and tan δ with temperature for DNR/NC-0 and the NC-filled composite DNR/NC-2. The maximum storage modulus values recorded were 3128 MPa for DNR/NC-0 and 3845 MPa for DNR/NC-2, indicating increased stiffness upon NC incorporation [41]. The corresponding loss modulus vs. temperature curves reveals the glass transition temperatures (T_g) of the samples, determined from the peak positions. The T_g values of DNR/NC-0 and DNR/NC-2 were –52.24 °C and –51.35 °C, respectively, showing only a slight shift, suggesting that NC addition has minimal effect on the glass transition behavior of NR. The tan δ (E″/E′), which reflects the damping properties of the composites, also provides Tg values at the peak. A slight increase in Tg from –42.62°C for DNR/NC-0 to –41.56°C for DNR/NC-2 was observed with 2phr NC loading [42]. This upward shift implies good interfacial interaction between NC and NR chains, likely due to the nucleation, size, and surface effects of NC. Overall, these findings suggest improved mechanical properties and filler–matrix interaction, with negligible impact on the thermal transition behavior of NR. The tan δ values at 0°C and 60°C are commonly used to evaluate the wet-skid resistance and rolling resistance of rubber composites, respectively. For DNR/NC-0 and DNR/NC-2, the tan δ at 60°C was 0.041 and 0.043, while the tan δ at 0°C was 0.01 and 0.02, respectively. The higher tan δ values observed in DNR/NC-2 at both temperatures indicate improved wet traction along with the modest increase in rolling resistance [43,44]. These results suggest that the incorporation of NC enhances the dynamic mechanical performance of the composite, making it more suitable for tire-related applications.

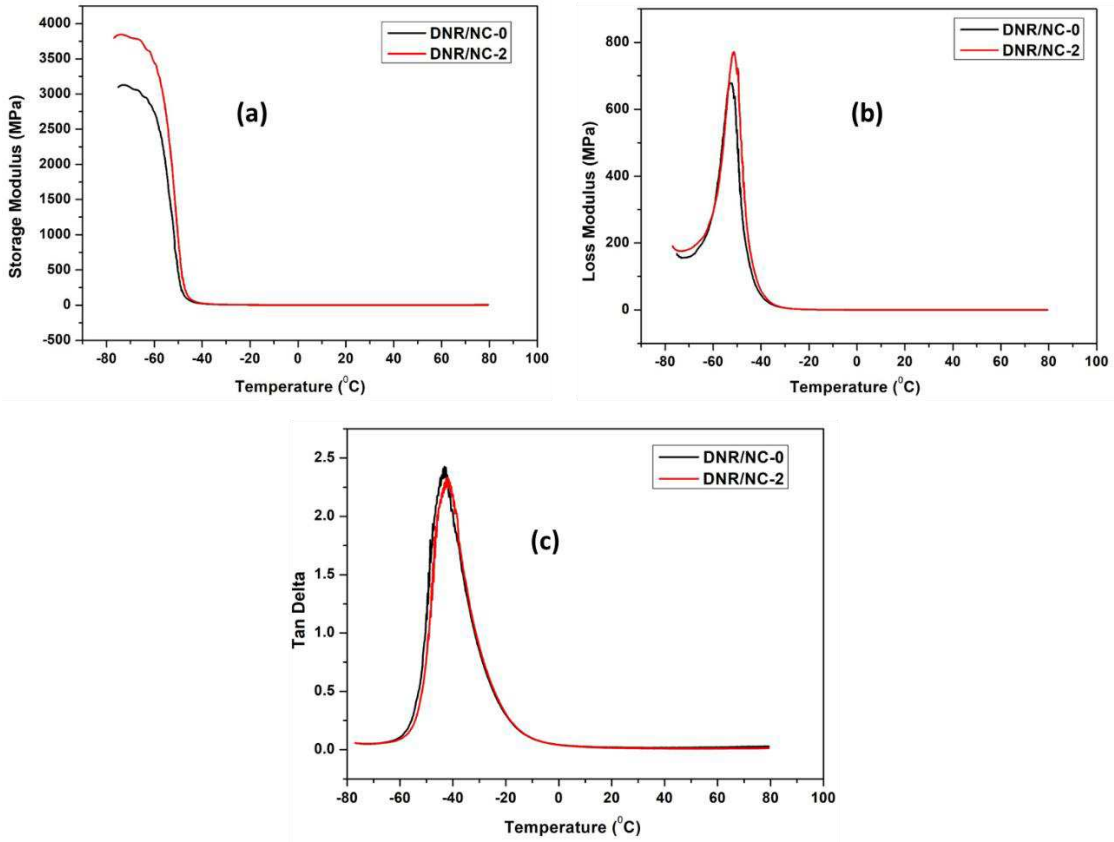


Fig. 9 (a) Storage modulus, (b) loss modulus and (c) tan δ as a function of temperature for DNR/NC-0 and the DNR/NC-2 composite

3.2.11 Swelling Studies

The swelling index and crosslink density values of DNR composites are provided in Table 7. All the composites exhibited a rapid increase in solvent uptake during the initial swelling stage, which gradually slowed and eventually reached a plateau, indicating equilibrium swelling [45]. In the early phase, the polymer matrix is more accessible to solvent molecules due to the relatively unconstrained nature of the rubber chains, allowing easier diffusion. However, as the NC content increases, solvent absorption in the DNR composites decreases. This reduction is attributed to the uniform dispersion of NC in the matrix, which restricts the segmental mobility of the rubber chains and reduces the free volume available for solvent penetration. Additionally, the incorporation of NC contributes to an increase in crosslink density, likely due to its reinforcing effect, which promotes more efficient dispersion of curing agents and enhances interfacial bonding within the composite system [46].

Table 7 Diffusion characteristics of DNR composites

Name of sample	Crosslink density (10^{-5} mol/g)	Swelling index (%)
DNR/NC-0	5.32±0.18	385±6
DNR/NC -1	6.06±0.16	374±9
DNR/NC-2	7.31±0.14	348±9
DNR/NC-3	6.59±0.13	359±8
DNR/NC-4	5.98±0.14	363±4
DNR/NC-5	5.84±0.21	377±8

3.2.12 Thermal analysis

The thermal decomposition characteristics of DNR/NC-0 and DNR/NC-2 composites are shown in Table 8 and Fig.10. The onset degradation temperature (T_{on}) for DNR/NC-0 was 317°C, while DNR/NC-2 exhibited a higher T_{on} of 325°C. This improvement indicates that NC acts as an effective reinforcing filler, promoting stronger interactions with the DNR matrix and thereby delaying the onset of thermal degradation [47,48]. The increase in T_{50} (temperature at 50% weight loss) observed for DNR/NC-2 is attributed to the barrier and reinforcement effects of NC, which slow down the degradation process and enhance thermal stability. Similarly, T_{max} was higher for DNR/NC-2, indicating improved resistance to thermal decomposition [49]. NC also contributes to more uniform heat dissipation and a delayed degradation profile. Moreover, the increased char residue at 650 °C for DNR/NC-2 suggests the formation of a thermally stable char layer that acts as a protective barrier, reducing further degradation and enhancing the composite's overall thermal resistance.

Table 8 Data on thermal degradation

Sample name	Onset degradation temperature (°C)	Temperature at 50% degradation (°C)	Maximum degradation temperature (°C)	Residue at 650°C
DNR/NC-0	317	387	383	3.98
DNR/NC-2	325	388	384	4.30

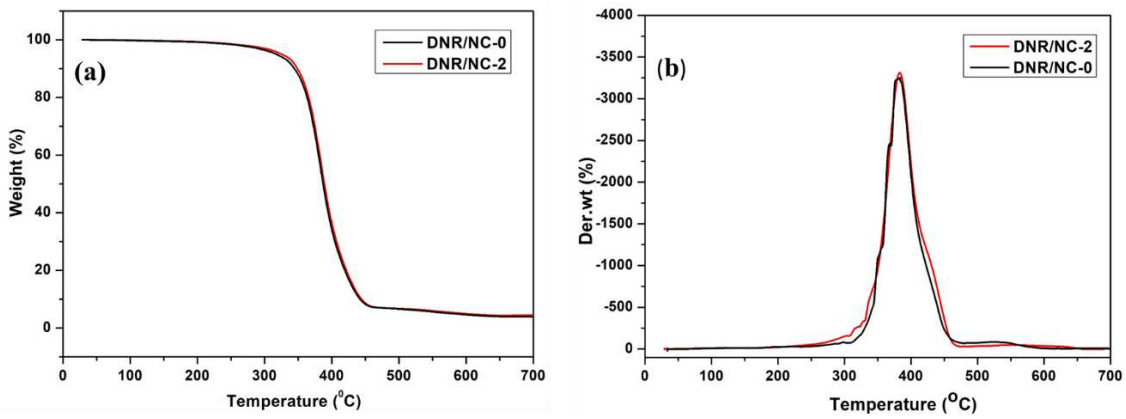


Fig. 10 (a) TG and (b) DTG curves of DNR/NC-0 and the DNR/NC-2 composite

3.2.13 Kinetic analysis

The kinetic parameters of the DNR/NC-0, DNR/NC-2 and DNR/NC-5 composites were determined using four iso-conversional models: FWO, KAS, Friedman, and Vyazovkin, at a conversion range (α) from 0.1 to 0.8. The activation energy (E_a) and pre-exponential factor (A) were calculated, across heating rates of 10, 15, 20 and 25°C/min. As demonstrated in Table 9, all samples displayed uniform degradation patterns when analyzed using the different kinetic models.

Table 9 The E_a and A values of FWO, KAS, Vyazovkin and Friedman models for DNR/NC-0, DNR/NC-2, and DNR/NC-5 composites

	FWO		**KAS**		**Friedman**		**Vyazovkin**	
α	E_a (kJ/mol)	A (s^{-1})	E_a (kJ/mol)	A (s^{-1})	E_a (kJ/mol)	A (s^{-1})	E_a (kJ/mol)	A (s^{-1})
	DNR/NC-0							
	R^2 =0.9992		R^2 =0.9227		R^2 =0.9955		R^2 =0.9991	
0.1	126.67	1.16×10^{8}	126.46	1.08×10^{8}	141.34	1.72×10^{9}	129.36	1.52×10^{8}
0.2	133.60	3.84×10^{8}	133.39	3.62×10^{8}	142.33	2.1×10^{9}	134.87	4.76×10^{8}
0.3	135.65	5.6×10^{8}	135.44	5.26×10^{8}	149.83	8.77×10^{9}	142.00	1.91×10^{9}
0.4	139.66	1.19×10^{9}	139.45	1.14×10^{9}	155.66	2.51×10^{10}	150.59	9.44×10^{9}
0.5	144.11	2.72×10^{9}	143.89	2.61×10^{9}	170.64	3.52×10^{11}	161.48	6.44×10^{10}
0.6	153.44	1.46×10^{10}	153.23	1.44×10^{10}	196.12	2.77×10^{13}	190.03	9.14×10^{12}
0.7	174.90	6.34×10^{11}	174.71	6.65×10^{11}	243.21	7.57×10^{16}	239.65	4.01×10^{16}
0.8	252.98	5.25×10^{17}	252.83	5.61×10^{17}	325.02	1.87×10^{30}	301.62	3.66×10^{31}
	DNR/NC-2							
	R^2 =1.0000		R^2 =1.0000		R^2 =0.9973		R^2 =0.9961	
0.1	124.93	6.36×10^{7}	124.60	5.83×10^{7}	137.39	6.31×10^{8}	135.57	4.44×10^{8}
0.2	151.29	9.59×10^{9}	151.03	9.77×10^{9}	177.92	1.61×10^{12}	181.32	2.99×10^{12}
0.3	170.38	3.54×10^{11}	170.16	3.78×10^{11}	207.45	3.9×10^{14}	194.37	3.27×10^{13}
0.4	187.19	8.07×10^{12}	186.99	8.83×10^{12}	230.82	2.56×10^{16}	215.04	1.32×10^{15}
0.5	205.69	2.37×10^{14}	205.51	2.62×10^{14}	257.18	2.44×10^{18}	249.19	5.6×10^{17}
0.6	235.04	4.75×10^{16}	234.88	5.21×10^{16}	302.19	5.53×10^{21}	295.83	1.75×10^{21}
0.7	286.96	4.9×10^{20}	286.83	4.94×10^{20}	379.28	2.56×10^{27}	371.74	6.68×10^{26}
0.8	419.22	6.44×10^{30}	419.13	4.12×10^{30}	569.46	2.14×10^{41}	539.12	1.05×10^{39}
	DNR/NC-5							
	R^2 =0.9980		R^2 =0.9995		R^2 =0.9988		R^2 =0.9978	
0.1	128.21	1.38×10^{8}	128.13	1.28×10^{8}	161.84	8.71×10^{10}	155.20	2.29×10^{10}
0.2	151.75	1.16×10^{10}	151.55	1.18×10^{10}	183.64	5.24×10^{12}	174.89	9.25×10^{11}
0.3	166.51	1.88×10^{11}	166.33	1.98×10^{11}	197.93	7.69×10^{13}	186.27	8.2×10^{12}
0.4	178.64	1.82×10^{12}	178.46	1.95×10^{12}	216.09	2.03×10^{15}	213.07	1.09×10^{15}
0.5	190.59	1.62×10^{13}	190.42	1.76×10^{13}	234.85	5.22×10^{16}	228.93	1.72×10^{16}
0.6	204.72	2.04×10^{14}	204.56	2.23×10^{14}	261.12	4.44×10^{18}	244.33	2.07×10^{17}
0.7	229.39	1.56×10^{16}	229.24	1.7×10^{16}	284.29	1.58×10^{20}	283.43	1.35×10^{20}
0.8	279.22	8.22×10^{19}	279.09	8.43×10^{19}	361.98	5.24×10^{25}	346.47	3.4×10^{24}

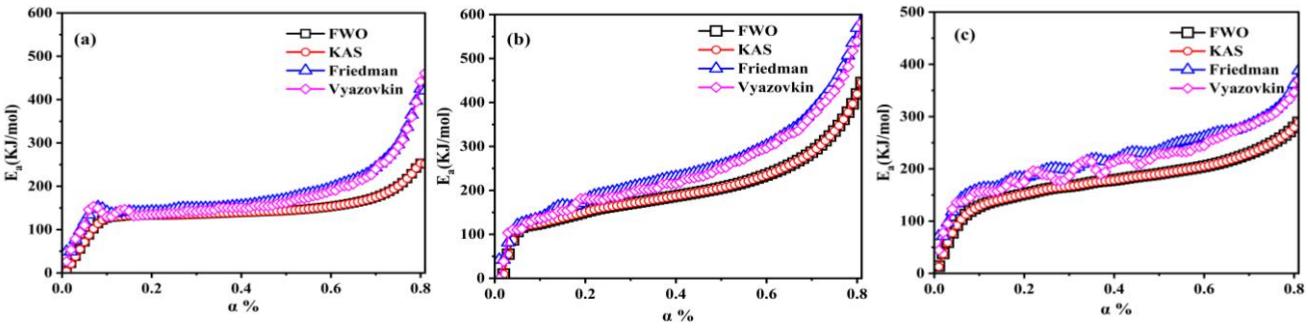


Fig. 11 E_a vs. α profiles of (a) DNR/NC-0 (b) DNR/NC-2 composite and (c) DNR/NC-5 by different kinetic models

The variation of E_a with α for DNR/NC-0, DNR/NC-2, and DNR/NC-5 is illustrated in Fig. 11. The observed non-linearity in the E_a values suggests that the decomposition of the developed composite proceeds via multistep kinetics [50]. In all analyzed samples, E_a exhibited an increase with α, reaching a peak at α = 0.8. The initial low value of E_a can be primarily attributed to the processes of moisture evaporation and the cleavage of weaker bonds. As α increased, E_a exhibited a continuous increase, indicative of the progressive thermal degradation occurring within both the NR matrix and the NC filler, and reached the maximum at α=0.8,which corresponds to char formation, char oxidation, and the final decomposition stages [51]. The E_a values of DNR/NC-0, as determined by the FWO, KAS, Friedman and Vyazovkin models are 126-252 ,126-252 ,141-325,129-301 KJ/mol, respectively. For DNR/NC-2, the E_a values obtained from the FWO, KAS, Friedman and Vyazovkin models ranged from 124-419,124-419,137-569 ,135-539 KJ/mol, while the E_a values for DNR/NC-5 ranged from 128-279, 128-279,161-361, and 155-346 KJ/mol, respectively.

As previously reported, the Friedman and Vyazovkin approaches produced much higher E_a values, whereas the FWO and KAS methods produced equal values [52]. The FWO and KAS models isoconversional methods are based on similar principles. In contrast, the Friedman model represents a differential isoconversional approach. The Vyazovkin model represents a sophisticated integral approach, exhibiting sensitivity to the reaction mechanism as well as discrepancies in experimental outcomes [53]. Additionally, all four models' R^2 values showed a higher correlation at each conversion level, suggesting that the computed E_a values were more accurate and reliable.

All the NC-reinforced composites showed higher E_a values than the DNR/NC-0 at advanced conversion stages, indicating improved thermal stability. The DNR/NC-2 composite showed a sharper increase from 137 to 569 kJ/mol over the same conversion range, indicating stronger matrix–filler interactions that demand higher decomposition energy. The DNR/NC-5

composite also exhibited a reinforcing effect, with E_a increasing from 161 to 361 kJ/mol. However, its E_a values were lower than the DNR/NC-2.This suggests that NC reinforcement is most effective at moderate loadings before potential filler agglomeration occurs [52]. The A values ranged from 10^8–10^{17} s^{-1} for DNR/NC-0, 10^7–10^{30} s^{-1} for DNR/NC-2, and 10^8–10^{19} s^{-1} for DNR/NC-5, indicating increased reaction complexity at higher conversion levels [54].

4. Conclusion

The present study demonstrated that NC incorporation significantly influenced the performance of DNR/NC nanocomposites. Among the formulations studied, DNR/NC-2 exhibited stable enhancement in mechanical, thermal, tribological, and physicochemical properties due to effective filler dispersion and stronger interfacial interactions. Thermal degradation kinetics indicated improved E_a for NC filled nanocomposites, confirming enhanced thermal resistance. In contrast, higher NC loading inversely affected nanocomposite performance due to agglomeration effects. These findings establish moderate NC loading as an effective strategy for developing sustainable DNR/NC nanocomposites with improved multifunctional properties and potential biomedical applications.

Credit author statement

Poornima M P: Conceptualization, Data curation, Formal analysis, Investigation, Methodology

and Writing – original draft; Roshna M: Data curation, Methodology and Writing – original draft; Dileep P: Resources, Supervision, Visualization and Writing – review & editing; Sinto Jacob: Conceptualisation, Data curation, Supervision, validation and Writing – review & editing.

Declaration of interest

The authors declare that they have no known competing financial interests or personal relationships that could have appeared to influence the work reported in this paper.

Funding

No external funding was provided for this work.

References

[1] M.M. Rahman, K.H. Khan, M.M.H. Parvez, N. Irizarry, M.N. Uddin, Polymer Nanocomposites with Optimized Nanoparticle Dispersion and Enhanced Functionalities for Industrial Applications, Processes 13 (2025). https://doi.org/10.3390/pr13040994.

[2] L. Bokobza, Elastomer Nanocomposites : Effect of Filler – Matrix and Filler – Filler Interactions, Polymers 15 (2023). https://doi.org/https://doi.org/10.3390/polym15132900.

[3] M. Dadkhah, M. Messori, A comprehensive overview of conventional and bio-based fillers for rubber formulations sustainability, Materials Today Sustainability 27 (2024) 100886. https://doi.org/10.1016/j.mtsust.2024.100886.

[4] B. Hajare, R.K. Shuib, A comprehensive review on rubber-based adhesives, Journal of Adhesion Science and Technology 39 (2025) 1133–1180. https://doi.org/10.1080/01694243.2024.2447456.

[5] M.F. Omar, F. Ali, M.S. Jami, A.S. Azmi, F. Ahmad, M.Z. Marzuki, S.K. Muniyandi, Z. Zainudin, M.P. Kim, A Comprehensive Review of Natural Rubber Composites: Properties, Compounding Aspects, and Renewable Practices with Natural Fibre Reinforcement, Journal of Renewable Materials 13 (2025) 497–538. https://doi.org/10.32604/jrm.2024.057248.

[6] J. Zhu, C. Abeykoon, N. Karim, Investigation into the effects of fillers in polymer processing, International Journal of Lightweight Materials and Manufacture 4 (2021) 370–382. https://doi.org/10.1016/j.ijlmm.2021.04.003.

[7] D.E. El Nashar, A.I. Khalaf, A review on reinforcing rubber goods for different valuable applications, Egyptian Journal of Chemistry 66 (2023) 503–529. https://doi.org/10.21608/EJCHEM.2022.173291.7164.

[8] S.K. Thomas, J. Parameswaranpillai, S. Krishnasamy, P.M.S. Begum, D. Nandi, S. Siengchin, J.J. George, N. Hameed, N. V. Salim, N. Sienkiewicz, A comprehensive review on cellulose, chitin, and starch as fillers in natural rubber biocomposites, Carbohydr. Polym. Technol. Appl. 2 (2021) 100095. https://doi.org/10.1016/j.carpta.2021.100095.

[9] J. Verma, M. Petru, S. Goel, Cellulose based materials to accelerate the transition towards sustainability, Industrial Crops and Products 210 (2024) 118078.

https://doi.org/10.1016/j.indcrop.2024.118078.

[10] A. Poulose, J. Parameswaranpillai, J.J. George, J.A. Gopi, S. Krishnasamy, M. Dominic C. D, N. Hameed, N. V. Salim, S. Radoor, N. Sienkiewicz, Nanocellulose: A Fundamental Material for Science and Technology Applications, Molecules 27 (2022) 1–27. https://doi.org/10.3390/molecules27228032.

[11] S. Antony Jose, N. Cowan, M. Davidson, G. Godina, I. Smith, J. Xin, P.L. Menezes, A Comprehensive Review on Cellulose Nanofibers, Nanomaterials, and Composites: Manufacturing, Properties, and Applications, Nanomaterials 15 (2025) 1–33. https://doi.org/10.3390/nano15050356.

[12] A. Babaei-Ghazvini, R. Patel, B. Vafakish, A.F.A. Yazdi, B. Acharya, Nanocellulose in targeted drug delivery: A review of modifications and synergistic applications, International Journal of Biological Macromolecules 278 (2024) 135200. https://doi.org/10.1016/j.ijbiomac.2024.135200.

[13] X. Yang, S.K. Biswas, J. Han, S. Tanpichai, M.C. Li, C. Chen, S. Zhu, A.K. Das, H. Yano, Surface and Interface Engineering for Nanocellulosic Advanced Materials, Advanced Materials 33 (2021). https://doi.org/10.1002/adma.202002264.

[14] V. Thakur, A. Guleria, S. Kumar, S. Sharma, K. Singh, Recent advances in nanocellulose processing, functionalization and applications: A review, Materials Advances 2 (2021) 1872–1895. https://doi.org/10.1039/d1ma00049g.

[15] M. Ghasemlou, F. Daver, E.P. Ivanova, Y. Habibi, B. Adhikari, Surface modifications of nanocellulose: From synthesis to high-performance nanocomposites, Progress in Polymer Science 119 (2021) 101418. https://doi.org/10.1016/j.progpolymsci.2021.101418.

[16] U. Ray, S. Zhu, Z. Pang, T. Li, Mechanics Design in Cellulose-Enabled High-Performance Functional Materials, Advanced Materials 33 (2021). https://doi.org/10.1002/adma.202002504.

[17] M. Dominic, R. Joseph, P.M. Sabura Begum, B.P. Kanoth, J. Chandra, S. Thomas, Green tire technology: Effect of rice husk derived nanocellulose (RHNC) in replacing carbon black (CB) in natural rubber (NR) compounding, Carbohydrate Polymers 230 (2020) 115620. https://doi.org/10.1016/j.carbpol.2019.115620.

[18] N. Koeipudsa, P. Phinyocheep, Cellulose nanocrystals from oil palm trunk biomass as a bio-reinforcing filler for improved mechanical properties of modified natural rubber composites, Polymer Composites 45 (2024) 4524–4537. https://doi.org/10.1002/pc.28078.

[19] N. Suppanucroa, A. Nimpaiboon, K. Boonchuay, A. Khamkeaw, M. Phisalaphong, Green composite sponge of natural rubber reinforced with cellulose filler using alginate as a dispersing agent, Journal of Materials Research and Technology 27 (2023) 3119–3130. https://doi.org/10.1016/j.jmrt.2023.10.139.

[20] M.P. Poornima, M. Anu Anie, P. Dileep, J. Sinto, Synthesis of nanocellulose from Acalypha hispida leaves through enzymatic hydrolysis, Int. J. Biol. Macromol. 26 (2024) 1–2. https://doi.org/10.1016/S0141-8130(99)00101-4.

[21] I. Meshram, T. Bhattacharjee, S. Sahoo, Enhancing Mechanical and Thermal Properties of Natural Rubber Composites via Nanocellulose Reinforcement from Coconut Shell Waste: A Sustainable Approach, International Journal of Advanced Research in Chemical Science 11 (2024) 25–36. https://doi.org/10.20431/2349-0403.1101003.

[22] H. Kazemi, F. Mighri, D. Rodrigue, A Review of Rubber Biocomposites Reinforced with Lignocellulosic Fillers, Journal of Composites Science 6 (2022). https://doi.org/10.3390/jcs6070183.

[23] S.K. Thomas, P. Dileep, P.M.S. Begum, Green polymer nanocomposites based on natural rubber and nanocellulose whiskers from Acacia caesia: Mechanical, thermal, and diffusion properties, Materials Today: Proceedings 51 (2022) 2444–2449. https://doi.org/10.1016/j.matpr.2021.11.613.

[24] N. George, G.A. Varghese, R. Joseph, Improved mechanical and barrier properties of natural rubber- multiwalled carbon nanotube composites with segregated network structure, Materials Today: Proceedings 9 (2019) 13–20. https://doi.org/10.1016/j.matpr.2019.02.030.

[25] P.M. Visakh, S. Thomas, K. Oksman, A.P. Mathew, Crosslinked Natural Rubber Nanocomposites Reinforced with Cellulose Whiskers Isolated from Bamboo Waste: Processing and Mechanical/Thermal Properties, Composites, Part A 43 (2012) 735.

[26] P. Dileep, S.K. Narayanankutty, Styrenated phenol modified nanosilica for improved

thermo-oxidative and mechanical properties of natural rubber, Polym. Test. 82 (2020) 106302. https://doi.org/10.1016/j.polymertesting.2019.106302.

[27] P. Yu, H. He, Y. Jia, S. Tian, J. Chen, D. Jia, Y. Luo, A comprehensive study on lignin as a green alternative of silica in natural rubber composites, Polymer Testing 54 (2016) 176–185. https://doi.org/10.1016/j.polymertesting.2016.07.014.

[28] P. Dileep, S. Jacob, C.S.J. Chandra, C.D.M. Dominic, M.P. Poornima, J.P. Rappai, S.K. Narayanankutty, Functionalized Nanosilica for Vulcanization Efficiency and Mechanical Properties of Natural Rubber Composites, Silicon 14 (2022) 4411–4422. https://doi.org/10.1007/s12633-021-01281-3.

[29] S. Mishra, N.G. Shimpi, Studies on mechanical, thermal, and flame retarding properties of polybutadiene rubber (PBR) nanocomposites, Polymer - Plastics Technology and Engineering 47 (2008) 72–81. https://doi.org/10.1080/03602550701580987.

[30] G.A. Varghese, S.K.N. , Dileep P, Journal of Advanced Scientific Research, … of Advanced Scientific … 1 (2021) 19–23. http://www.sciensage.info/journal/1359303580JASR_3006121.pdf.

[31] M. Dominic, R. Joseph, P.M.S. Begum, A.S. Kumar, P.A. Jeemol, T. Jose, D. Padmanabhan, K. Formela, S. Siengchin, J. Parameswaranpillai, M.R. Saeb, Cellulosic bionanocomposites based on acrylonitrile butadiene rubber and Cuscuta reflexa: adjusting structure-properties balance for higher performance, Cellulose 28 (2021) 7053–7073. https://doi.org/10.1007/s10570-021-03958-9.

[32] S. Vishvanathperumal, S. Gopalakannan, Effects of the Nanoclay and Crosslinking Systems on the Mechanical Properties of Ethylene-propylene-diene Monomer/styrene Butadiene Rubber Blends Nanocomposite, Silicon 11 (2019) 117–135. https://doi.org/10.1007/s12633-018-9836-x.

[33] P. Dileep, S.K. Narayanankutty, A novel method for preparation of nanosilica from bamboo leaves and its green modification as a multi-functional additive in styrene butadiene rubber, Materials Today Communications 24 (2020) 100957. https://doi.org/10.1016/j.mtcomm.2020.100957.

[34] P. Dileep, M.P. Poornima, S. Jacob, J.P. Rappai, C.D. Midhun Dominic, Accelerator functionalized nanosilica for vulcanization efficiency and thermal resistance of SBR,

Materials Today: Proceedings 51 (2022) 2599–2603. https://doi.org/10.1016/j.matpr.2021.12.568.

[35] C.K. Hong, H. Kim, C. Ryu, C. Nah, Y. Il Huh, S. Kaang, Effects of particle size and structure of carbon blacks on the abrasion of filled elastomer compounds, Journal of Materials Science 42 (2007) 8391–8399. https://doi.org/10.1007/s10853-007-1795-3.

[36] N. Rattanasom, T. Saowapark, C. Deeprasertkul, Reinforcement of natural rubber with silica/carbon black hybrid filler, Polymer Testing 26 (2007) 369–377. https://doi.org/10.1016/j.polymertesting.2006.12.003.

[37] V.D. Chari, D.V.S.G.K. Sharma, P.S.R. Prasad, S.R. Murthy, Dependence of thermal conductivity in micro to nano silica, Bulletin of Materials Science 36 (2013) 517–520. https://doi.org/10.1007/s12034-013-0519-3.

[38] C. Zhang, T. Zhai, R. Sabo, C. Clemons, Y. Dan, L.S. Turng, Reinforcing natural rubber with cellulose nanofibrils extracted from bleached eucalyptus kraft pulp, Journal of Biobased Materials and Bioenergy 8 (2014) 317–324. https://doi.org/10.1166/jbmb.2014.1441.

[39] S. Gunasekaran, R.K. Natarajan, A. Kala, FTIR spectra and mechanical strength analysis of some selected rubber derivatives, Spectrochimica Acta - Part A: Molecular and Biomolecular Spectroscopy 68 (2007) 323–330. https://doi.org/10.1016/j.saa.2006.11.039.

[40] G. Supanakorn, S. Taokaew, M. Phisalaphong, Ternary composite films of natural rubber, cellulose microfiber, and carboxymethyl cellulose for excellent mechanical properties, biodegradability and chemical resistance, Cellulose 28 (2021) 8553–8566. https://doi.org/10.1007/s10570-021-04082-4.

[41] S. Mitra, S. Chattopadhyay, A.K. Bhowmick, Studies of reinforcement behavior of unique elastomer-based nanocomposite gels, Polymer Composites 32 (2011) 103–113. https://doi.org/10.1002/pc.21025.

[42] N.R. Singha, M. Mahapatra, M. Karmakar, P.K. Chattopadhyay, Processing, characterization and application of natural rubber based environmentally friendly polymer composites, 2019. https://doi.org/10.1007/978-3-030-05399-4_29.

[43] A. Lang, M. Klüppel, Influences of temperature and load on the dry friction behaviour of tire tread compounds in contact with rough granite, Wear 380–381 (2017) 15–25. https://doi.org/10.1016/j.wear.2017.02.047.

[44] D. Gabriel, A. Karbach, D. Drechsler, J. Gutmann, Bound rubber morphology and loss tangent properties of carbon-black-filled rubber compounds, (2016) 501–511. https://doi.org/10.1007/s00396-015-3802-6.

[45] A.P. Haseena, K.P. Dasan, R. Namitha, G. Unnikrishna, S.A. Thomas, Investigation on interfacial adhesion of short sisal/coir hybrid fibre reinforced natural rubber composites by restricted equilibrium swelling technique, Composite Interfaces 11 (2004) 489–513. https://doi.org/10.1163/1568554042722955.

[46] S.K. Thomas, P.M.S. Begum, P. Dileep, K. V. Neenu, D.A. David, A. Santu, C.D. Midhun Dominic, Composites of resorcinol and hexamethylenetetramine modified nanocellulose whiskers as potential biofiller in natural rubber latex: synthesis, characterization and property evaluation, Biomass Convers. Biorefin. 14 (2024) 16769–16785. https://doi.org/10.1007/s13399-023-03850-5.

[47] J. Bras, M.L. Hassan, C. Bruzesse, E.A. Hassan, N.A. El-Wakil, A. Dufresne, Mechanical, barrier, and biodegradability properties of bagasse cellulose whiskers reinforced natural rubber nanocomposites, Industrial Crops and Products 32 (2010) 627–633. https://doi.org/10.1016/j.indcrop.2010.07.018.

[48] E. Abraham, M.S. Thomas, P. Deepalekshmi, B. Deepa, L.A. Pothen, S. Thomas, Biofiber-reinforced Natural Rubber Composites: Mechanical, Thermal and Biodegradation Properties, (2014) 105–118. https://doi.org/10.1142/9789814566469_0054.

[49] P.G. Gan, S.T. Sam, M.F. bin Abdullah, M.F. Omar, Thermal properties of nanocellulose-reinforced composites: A review, Journal of Applied Polymer Science 137 (2020). https://doi.org/10.1002/app.48544.

[50] S. Vyazovkin, N. Sbirrazzuoli, Isoconversional Kinetic Analysis of Thermally Stimulated Processes in Polymers, (2006) 1515–1532. https://doi.org/10.1002/marc.200600404.

[51] P. Bashpa, K. Bijudas, T. Francis, Solvent transport behavior and thermal degradation

kinetics of condom industry waste reinforced natural rubber composites, Thermal Advances 2 (2025) 100019. https://doi.org/10.1016/j.thradv.2024.100019.

[52] A. Jagtap, S.R. Kalbande, Investigation on pyrolysis kinetics and thermodynamic parameters of soybean straw : a comparative study using model - free methods, Biomass Conversion and Biorefinery (2021). https://doi.org/10.1007/s13399-021-02228-9.

[53] A. Fernandez, L. Rodriguez, D. Asensio, R. Rodriguez, G. Mazza, I.D.I. Química, F.D.I. Unsj, G. Vinculado, S. Juan, Journal of Environmental Chemical Engineering Kinetic analysis and thermodynamics properties of air / steam gasification of agricultural waste, Journal of Environmental Chemical Engineering 8 (2020) 103829. https://doi.org/10.1016/j.jece.2020.103829.

[54] P. Parthasarathy, A. Fernandez, D. Kumar, T. Al-ansari, H.R. Mackey, R. Rodriguez, G. Mazza, J. Vachan, G. Mckay, Thermogravimetric analysis of camel dung , date stone , and their blend for pyrolytic , kinetic , and thermodynamic studies, Cleaner Chemical Engineering 4 (2022) 100072. https://doi.org/10.1016/j.clce.2022.100072.